Optics Letters

Efficient generation of femtosecond millijoule pulses at 3.1 μm

Fangjie Zhou, Yi Wu, Alphonse Marra, and Zenghu Chang*

Institute for the Frontier of Attosecond Science and Technology, The College of Optics and Photonics (CREOL) and Department of Physics, University of Central Florida, Orlando, FL, 32816, USA
**Corresponding author: Zenghu.Chang@ucf.edu*

Received 8 September 2022; revised 18 October 2022; accepted 22 October 2022; posted 28 October 2022; published 15 November 2022

3.2-mJ, 92-fs pulses centered at 3.1 μm are generated at a 1-kHz repetition rate through a tabletop optical parametric chirped pulse amplification (OPCPA) system based on $ZnGeP_2$ crystals. Pumped by a 2-μm chirped pulse amplifier with a flat-top beam profile, the amplifier achieves a 16.5% overall efficiency, which, to the best of our knowledge, is the highest efficiency achieved by OPCPA at this wavelength. Harmonics up to the seventh order are observed after focusing the output in the air.

https://doi.org/10.1364/OL.474741

The development of ultrafast sources with high pulse energies and long wavelengths is the top demand of many strong-field experiments such as those involving generating soft x-ray pulses with attosecond durations through high harmonic generation (HHG). As the single-atom cutoff photon energy of a high harmonic spectrum scales quadratically with the wavelength of the driving laser, a longer-wavelength driver is therefore beneficial to extending the spectral range [1–3]. For generating single isolated attosecond pulses, the carrier-envelope phase (CEP) of the driving laser needs to be stabilized. Attosecond pulses in the water window region (282–533 eV) have been generated from CEP-locked sources in the 1.7 μm to 2 μm region [4–6]. Time-resolved experiments have been demonstrated at the nitrogen K-edge (400 eV) [7] and the titanium L-edge (460 eV) with table-top attosecond x rays, but not at the oxygen K-edge (533 eV), since the photon flux was too low there. High-peak-power, high-average-power, few-cycle, and CEP-locked lasers at center wavelengths longer than 2 μm are needed to generate high-flux, attosecond x rays spanning the entire water window and beyond. In this Letter, we report an optical parametric chirped pulse amplification (OPCPA) system centered at 3.1 μm as a step toward meeting these requirements.

The limited choices of laser gain media for wavelengths of 3 μm and longer motivated the development of optical parametric chirped pulse amplifiers to cover this spectral region. $KTiOPO_4$ (KTP), $KTiOAsO_4$ (KTA), and $LiNbO_3$ (LNB) are regularly used to achieve millijoule-level pulses at 3 to 4 μm with 100-fs durations by pumping with 0.8-μm Ti and 1-μm Nd, Yb lasers [8–11]. OPCPAs pumped by Yb:CaF_2 and Nd:YAG lasers have been built to output 8- to 35-mJ, 20-Hz pulses at 3.9 μm [8–10]. A dual-chirped optical parametric amplifier (DC-OPA) that used LNB and was pumped at 800 nm by a 700-mJ laser was able to generate 10-Hz, 31-mJ pulses at 3.3 μm [11]. A similar configuration was employed to generate 10-Hz, 13.3-mJ pulses that were tunable from 3.3 to 3.9 μm and pumped by a 900-mJ Nd:YAG laser [12]. Unfortunately, the efficiency of these high-energy nonlinear amplifiers centered at 3 μm or longer and pumped by ∼1-μm lasers is typically low (<10%) due to the large quantum defect.

Another major limiting factor on the efficiency of OPCPAs is the back conversion of the signal and idler to the pump due to nonuniformities in intensity across the Gaussian-shaped temporal and spatial profiles. A more uniform spatial and temporal profile supports a much higher efficiency. Although a flat-top temporal profile can is difficult to achieve, diffraction optics have been reported that convert Gaussian beam profiles to top-hat ones. Applying this technique, a 1-μm-pumped OPCPA boosted its overall conversion efficiency from 5.4% to 10.2% [13,14].

In this work, we report an efficient 3.1-μm OPCPA based on $ZnGeP_2$ (ZGP) crystals that outputs multi-millijoule, 92-fs pulses to enable strong-field experiments. The OPCPA is pumped by a 2-μm laser, which reduces the quantum defect by half as compared with OPCPAs pumped by 1-μm lasers. The final-stage amplifier is pumped by a flap-top beam enabling an efficiency of 20%, which, to the best of our knowledge, exceeds all existing sources at the same wavelength.

The configuration of the OPCPA is shown in Fig. 1. It starts with a multi-pass Ti:sapphire chirped pulse amplifier (CPA) that produces 44-fs, 2-mJ pulses at 800 nm. The pulse energy is split in half to generate seed pulses for the 3.1-μm signal and the 2.05-μm pump of the OPCPA separately.

The wavelength of the pump laser for ZGP should be longer than 2 μm to reduce absorption. A Ho:YLF CPA that outputs 28-mJ, 6.4-ps pulses at 2.05 μm, seeded by a DC-OPA driven by 1-mJ pulses from the Ti:sapphire laser, has been developed [15–17]. The narrowband output of the DC-OPA allows a 5-μJ seed after being stretched by a chirped volume Bragg grating (CVBG) with a 4.5-nm bandwidth. The high pulse energy allows the seed to be pre-amplified to the mJ level in a double-pass configuration. After four stages of amplification, the pulse energy is boosted to 60 mJ. However, the difference between dn/dT along the a axis and that along the c axis of the Ho:YLF results in an elliptical beam shape at high pump power when the thermal lensing effect becomes significant. The group delay dispersion of the CVBG varies due to the non-uniform temperature distribution at high incident power, leading to a longer pulse [18].

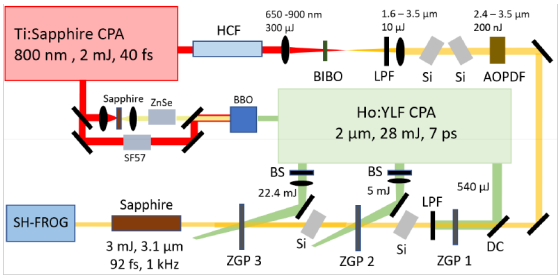

Fig. 1. Optical layout of the OPCPA consisting of a Ti:sapphire CPA, a gas-filled hollow-core fiber (HCF), an intra-pulse difference frequency generation (IP-DFG) unit, a Ho:YLF CPA, an AOPDF, and a three-stage ZGP-based optical parametric amplifier (OPA). BS: beam shaper, Si: silicon, LPF: long-pass filter.

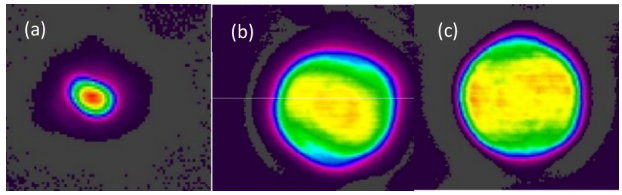

Fig. 2. Pump beam profiles of (a) the first stage (without the beam shaper), (b) the second stage, and (c) the third stage (with the beam shaper). The third-stage pump beam profile is the image of the original beam.

Because both the temporal duration and spatial beam profile are crucial to parametric amplification, the output pulse energy is limited to 28 mJ to balance pulse energy with spatial and temporal pulse quality while maintaining a 7-ps pulse duration.

The signal of the OPCPA is derived from the other half of the Ti:sapphire output. 1-mJ pulses at 800 nm are spectrally broadened to 650–900 nm in an argon-gas-filled hollow-core fiber (HCF). Then an octave-broad spectrum spanning 800 to 3500 nm is generated via intra-pulse difference frequency generation (IP-DFG) in a 0.8-mm-thick BiB_3O_6 (BIBO) crystal [19]. A bandpass filter is placed after the HCF to block the 800-nm light and decrease the pulse energy to 300 µJ to reduce the beam distortion caused by the filamentation in the air after the BIBO. IP-DFG yields 10-µJ pulses spanning 0.8 to 3.5 µm, although only the 2.4- to 3.5-µm portion of the spectrum serves as the signal at 2 µJ per pulse. The signal is temporally stretched by two 30-mm silicon windows, each providing 15,000 fs^2 of dispersion, and an acousto-optic programmable dispersive filter (AOPDF) with a 10% diffraction efficiency to 5 ps. The microjoule-level energy of the IP-DFG output allows the low-throughput AOPDF to be used to compensate for high-order phase errors. The AOPDF is much more compact than a phase compensator based on a spatial light modulator in a zero-dispersion grating compressor.

The 200-nJ signal is amplified in a three-stage ZGP OPCPA. To enable easy conversion between the signal scheme, in which the 3-µm signal is amplified, and the idler scheme, in which the 6-µm idler is generated and amplified, the first stage of the OPCPA employs a collinear configuration. A 2.4-µm or a 4.5-µm long-pass filter is placed after the first-stage ZGP to block the pump in the signal scheme or both the signal and the pump in the idler scheme, respectively. The output of the Ho:YLF laser is split into three beams by two beam splitters with 80% and 90% respectively. Out of 28 mJ of total pump energy, 0.56 mJ, 5 mJ, and 22.4 mJ are sent to the first, second, and third OPCPA stages, respectively.

Due to the Gaussian pulse shape of the pump and the phase-matching bandwidth of ZGP, the pulse is shortened to 3 ps after amplification. In order to maintain a temporal overlap between the signal and the pump, a 30-mm silicon window is placed after the first stage and another is placed after the second stage to stretch the signal to 5 ps. In addition, a beam shaper (HoLo/Or TH248) is applied to the second- and third-stage pump beams to convert their beam profiles from Gaussian to top hat. Since the input beam is not perfectly Gaussian, the input beam size and divergence are carefully adjusted to obtain a flat-top profile. Figure 2 shows the pump beam profiles for each stage. The distortion from the CVBG compressor and the thermal lens from the Ho:YLF reduce the beam quality, but the beam shaper is still able to provide a nearly flat-top beam profile.

It was found that the dispersion of the CVBG changes slightly in the vertical direction, which leads to pulse-front tilt. When amplified without the beam shaper, the delay between different portions of the pump results in spatial chirp in the vertical direction of the signal beam. However, as the beam is redistributed by the beam shaper, the spatial chirp is largely mitigated.

The signal is amplified to 35 µJ in the first stage in a 3-mm-thick ZGP crystal set at a 54° phase-matching angle, which is accompanied by a 15-µJ idler at 6 µm. The pump intensity is set to 1.6 GW/cm^2 to optimize the pulse energy and the spectrum. To eliminate beam distortion induced by multiphoton absorption of the long-pass filter, a small angle ($\alpha = 0.3°$) is introduced in the vertical direction between the pump and the signal, which allows the signal beam to be separated from the pump after a long optical path. Pumping with 1.3-GW/cm^2 intensity, the signal is further increased to 550 µJ in the second stage with a 2-mm-thick ZGP crystal. To ensure a uniform output and reduce back conversion at the center of the beam from the second stage, the $1/e^2$ beam diameter of the signal is enlarged to 7 mm, which is the same as that of the flat-top pump. The third stage employs a similar setup to the second stage: a 22.4-mJ pump with the same intensity as the second-stage pump is used to boost the signal to 4.6 mJ. Taking advantage of the large aperture size of the crystal (20×20 mm^2), the pump beam size is magnified to 16 mm in diameter with a 1.3-GW/cm^2 peak intensity. Although the amplified signal from the first stage is not flat top, the flat-top pump in the second stage transforms the signal to a flat-top profile. With seeding and pump beams both flat-shaped, the third stage reaches a conversion efficiency of 21%—about 6% higher than when a Gaussian pump and a Gaussian signal are used. The overall pump-to-signal efficiency of all three stages is 17.5%, surpassing all existing sources at the same wavelength (to the best of our knowledge). The flat-top beam profile of the pump also ensures a good beam profile for the final output, as shown in Fig. 3.

Numerical simulations of each stage of the OPCPA are performed using the *Hussar* code to understand the limiting factors on the pulse duration and pulse energy [20]. As shown in Fig. 4(a), the spectral bandwidth of the first-stage output is limited by the phase-matching bandwidth of the ZGP crystal at 3.1 µm. It is further narrowed through the second stage due to the use of a non-collinear configuration, as shown in Fig. 4(b). The transmission through the air is also shown in Fig. 4(b). The spacing between the absorption lines and the line widths are smaller

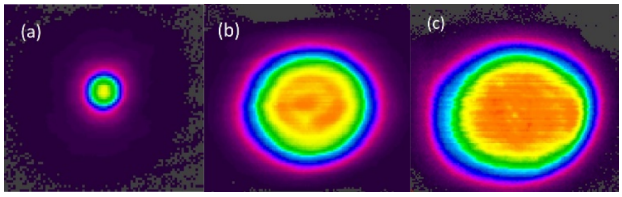

Fig. 3. Output signal beam profiles of (a) the first stage, (b) the second stage, and (c) the third stage at the far field.

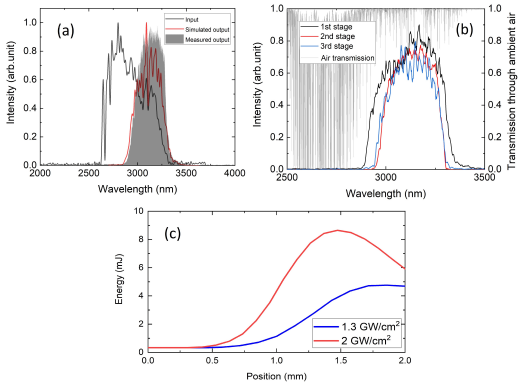

Fig. 4. (a) Input, simulated, and measured spectra after the first stage. (b) Spectrum after each stage and the transmission of a 2-m-long air path with 36% relative humidity at 24°C. (c) Simulated output energy versus crystal thickness for different pump intensities.

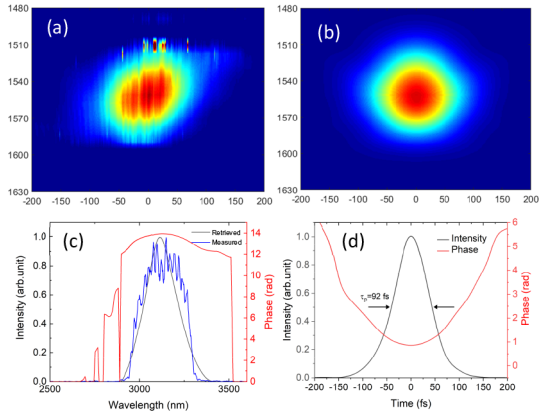

Fig. 5. (a) Measured and (b) retrieved FROG traces of the output pulse. (c) Retrieved intensity and the phase. (d) Measured and retrieved spectra.

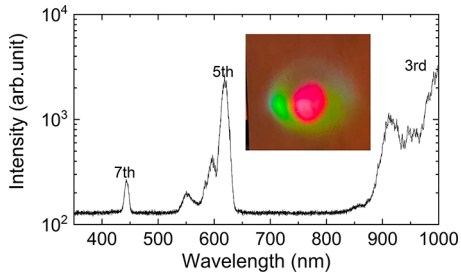

Fig. 6. Measured spectrum after filamentation in the air. Inset: the beam after the filament, measured with a CCD camera.

than the resolution of the scanning monochromator used in the measurements (2 nm, APE waveScan). It is thus expected that the discrete line absorptions do not change the global profile of the output spectrum. The modulation of the measured spectra is likely caused by power fluctuations of OPCPA output and the change in the thermal background during the scan. The Fourier limit prevents the pulse from being compressed to one or two cycles, as is possible for the 1.7-μm OPCPAs based on BIBO [6].

The simulated output pulse energy for each stage agrees well with the experimental result and reveals the potential for higher pulse energy. To prevent back conversion in the 2-mm crystal, the pump intensity for the third stage is maintained at 1.3 GW/cm^2, which is well below the damage threshold of ZGP [21,22]. The simulation predicts that the output energy may reach 9 mJ in the future by using a thinner crystal and a 36-mJ pump for the third stage (2 GW/cm^2), as shown in Fig. 4(c). This is feasible given the 60-mJ maximum output of the Ho:YLF laser.

The 4.6-mJ picosecond signal pulses after the third OPCPA stage are positively chirped. They are compressed by two passes through two pieces of 50-mm-long, AR-coated bulk sapphire with an overall throughput of 70%. The higher-order dispersion is managed by the AOPDF. Unfortunately, water condensation on the anti-reflection coating limits the transmission to 92% for each sapphire rod. Transmission may be improved by replacing the coating and reducing the number of reflections from the surfaces.

The compressed pulse is characterized by a second-harmonic frequency-resolved optical gating (SH-FROG) with a 100-μm-thick BBO crystal. Although BBO exhibits absorption for wavelengths longer than 2 μm, the thin crystal maintains 90% transmission at 3.1 μm. Figure 5 shows the measured and retrieved FROG traces and spectra. The retrieved 92-fs pulse duration is only slightly longer than the 90-fs Fourier limit. Shorter pulses can be obtained via nonlinear compression without a significant loss of energy in the future [23,24].

To explore the possibility of using the output pulse in a strong-field experiment, filamentation in the atmosphere is tested by focusing the beam using a variety of lenses with different focal lengths. The seventh harmonic is observed when an $f = 100$ mm lens is used, indicating a peak intensity of 12 TW/cm^2. The fundamental beam is blocked by two N-BK7 windows. The transmitted visible light is detected by a Photon Control SPM-002 spectrometer, and the spectrum is shown in Fig. 6. As the detection bandwidth of the spectrometer is from 350 to 1000 nm, only part of the third-order spectrum but the full fifth-order and seventh-order spectra are shown. The generation of up to seven harmonics is well-grounded evidence that the peak intensity of the OPCPA output is sufficient for many strong-field experiments.

In conclusion, we developed an OPCPA at 3 μm that outputs 3.2-mJ pulses with 92-fs duration based on ZGP. Pumped by a 2-μm Ho:YLF laser, the efficiency of the OPCPA is greatly improved in comparison to existing sources with 1-μm pumps. The use of beam shapers to convert the pump profile to a flattop further enhances the pulse energy, making it the highest-energy 3-μm ZGP-based OPCPA pumped at 2 μm to generate femtosecond pulses. This source was able to successfully generate harmonics to the seventh order in the atmosphere, indicating its potential to drive high harmonics beyond the water window

and toward the keV region. Even higher peak power and higher average power may be realizable by using larger pump energies and thinner ZGP crystals, which will impact the study of light filamentation in the 3- to 5-μm infrared atmospheric transmission window [25] and the development of high-dose-rate ionizing-radiation sources for radiation therapy [26].

Funding. National Science Foundation (2207674); Defense Threat Reduction Agency (HDTRA11910026); Air Force Office of Scientific Research (FA9550-20-1-0295).

Disclosures. The authors declare no conflicts of interest.

Data availability. Data underlying the results presented in this Letter are not publicly available at this time, but may be obtained from the authors upon reasonable request.

REFERENCES

1. P. B. Corkum, Phys. Rev. Lett. **71**, 1994 (1993).
2. K. Schafer, B. Yang, L. DiMauro, and K. Kulander, Phys. Rev. Lett. **70**, 1599 (1993).
3. B. Shan and Z. Chang, Phys. Rev. A **65**, 011804 (2001).
4. N. Ishii, K. Kaneshima, K. Kitano, T. Kanai, S. Watanabe, and J. Itatani, Nat. Commun. **5**, 3331 (2014).
5. S. Cousin, F. Silva, S. Teichmann, M. Hemmer, B. Buades, and J. Biegert, Opt. Lett. **39**, 5383 (2014).
6. J. Li, X. Ren, Y. Yin, K. Zhao, A. Chew, Y. Cheng, E. Cunningham, Y. Wang, S. Hu, Y. Wu, M. Chini, and Z. Chang, Nat. Commun. **8**, 186 (2017).
7. N. Saito, H. Sannohe, N. Ishii, T. Kanai, N. osugi, Y. Wu, A. Chew, S. Han, Z. Chang, and J. Itatani, Optica **6**, 1542 (2019).
8. G. Andriukaitis, T. Balčiūnas, S. Ališauskas, A. Pugžlys, A. Baltuška, T. Popmintchev, M.-C. Chen, M. M. Murnane, and H. C. Kapteyn, Opt. Lett. **36**, 2755 (2011).
9. A. V. Mitrofanov, A. A. Voronin, D. A. Sidorov-Biryukov, S. I. Mitryukovsky, A. B. Fedotov, E. E. Serebryannikov, D. V. Meshchankin, V. Shumakova, S. Ališauskas, A. Pugžlys, V. Ya. Panchenko, A. Baltuška, and A. M. Zheltikov, Optica **3**, 299 (2016).
10. Yuxi Fu, Bing Xue, Katsumi Midorikawa, and Eiji J. Takahashi, Appl. Phys. Lett. **112**, 241105 (2018).
11. K. Zhao, H. Zhong, P. Yuan, G. Xie, J. Wang, J. Ma, and L. Qian, Opt. Lett. **38**, 2159 (2013).
12. A. D. Shiner, C. Trallero-Herrero, N. Kajumba, H.-C. Bandulet, D. Comtois, F. Légaré, M. Giguère, J.-C. Kieffer, P. B. Corkum, and D. M. Villeneuve, Phys. Rev. Lett. **103**, 073902 (2009).
13. L. J. Waxer, V. Bagnoud, I. A. Begishev, M. J. Guardalben, J. Puth, and J. D. Zuegel, Opt. Lett. **28**, 1245 (2003).
14. X. Zou, W. Li, S. Qu, K. Liu, H. Li, Q. J. Wang, Y. Zhang, and H. Liang, Laser Photonics Rev. **15**, 2000292 (2021).
15. F. Zhou, A. Cintron, Y. Wu, and Z. Chang, Opt. Continuum **1**, 1060 (2022).
16. Y. Yin, X. Ren, Y. Wang, F. Zhuang, J. Li, and Z. Chang, Photonics Res. **6**, 1 (2018).
17. K. Murari, F. J. Zhou, Y. C. Yin, Y. Wu, B. Weaver, T. Avni, E. Larsen, and Z. Chang, Appl. Phys. Lett. **117**, 141102 (2020).
18. M. Smrž, J. Mužík, D. Štěpánková, H. Turčičová, O. Novák, M. Chyla, P. Hauschwitz, J. Brajer, J. Kubát, F. Todorov, and T. Mocek, OSA Continuum **4**, 940 (2021).
19. Y. Yin, X. Ren, A. Chew, J. Li, Y. Wang, F. Zhuang, Y. Wu, and Z. Chang, Sci. Rep. **7**, 11097 (2017).
20. T. M. Kardás, M. I. Nejbauer, P. I. Wnuk, B. Resan, C. I. Radzewicz, and P. Wasylczyk, Sci. Rep. **7**, 42889 (2017).
21. L. von Grafenstein, M. Bock, D. Ueberschaer, E. Escoto, A. Koç, K. Zawilski, P. Schunemann, U. Griebner, and T. Elsaesser, Opt. Lett. **45**, 5998 (2020).
22. U. Elu, T. Steinle, D. Sánchez, L. Maidment, K. Zawilski, P. Schunemann, U. D. Zeitner, C. Simon-Boisson, and J. Biegert, Opt. Lett. **44**, 3194 (2019).
23. G. Fan, T. Balčiūnas, T. Kanai, T. Flöry, G. Andriukaitis, B. E. Schmidt, F. Légaré, and A. Baltuška, Optica **3**, 1308 (2016).
24. P. Wang, Y. Li, W. Li, H. Su, B. Shao, S. Li, C. Wang, D. Wang, R. Zhao, Y. Peng, Y. Leng, R. Li, and Z. Xu, Opt. Lett. **43**, 2197 (2018).
25. A. V. Mitrofanov, A. A. Voronin, D. A. Sidorov-Biryukov, A. Pugžlys, E. A. Stepanov, G. Andriukaitis, T. Flöry, S. Ališauskas, A. B. Fedotov, A. Baltuška, and A. M. Zheltikov, Sci. Rep. **5**, 8368 (2015).
26. S. Vallières, J. Powell, T. Connell, M. Evans, S. Fourmaux, S. Payeur, P. Lassonde, F. Fillion-Gourdeau, S. MacLean, and F. Légaré, "High dose-rate ionizing radiation source from tight focusing in air of a mJ-class femtosecond laser," arXiv, arXiv:2207.05773 (2022).